Noname manuscript No.
(will be inserted by the editor)

Noise induced multistability in the square root map

Eoghan J. Staunton · Petri T. Piiroinen

This is a pre-print of an article accepted to be published in Nonlinear Dynamics in October 2018. DOI:10.1007/s11071-018-4595-1

Abstract The effects of small-amplitude additive Gaussian white noise on the one-dimensional square root map are investigated. In particular the focus is on the unexpected effects noise of varying amplitudes has on the system for parameter regions just outside intervals of multistability. It is shown that in these regions periodic behaviour that is unstable in the deterministic system can be effectively stabilised by the addition of noise of an appropriate amplitude. Features of noise-induced transitions from stable to stabilised unstable periodic behaviour are highlighted and it is shown how these features can be understood by examining relative levels of expansion and contraction in the deterministic map.

Keywords square root map · impacting systems · noise, period-adding bifurcations · multistability · noise-induced transitions

1 Introduction

An impact oscillator is a forced mechanical system that undergoes impacts at rigid stops. Many real-world mechanical systems including systems arising in engineering, for instance moored ships impacting a dock or rattling gears are modelled using impact oscillators [4]. It is important to understand such systems in order to avoid problems, such as wear and noise. In particular, since real-world systems, including mechanical systems, are subject to uncertainties, we must also investi-

Eoghan Staunton is supported by an Irish Research Council Postgraduate Scholarship, Award Number GOIPG/2015/3500.

EJ Staunton
School of Mathematics, Statistics and Applied Mathematics, National Univesity of Ireland, Galway
E-mail: eoghan.staunton@nuigalway.ie

PT Piiroinen
School of Mathematics, Statistics and Applied Mathematics, National Univesity of Ireland, Galway

gate how stochastic noise can affect such systems. In the case of impact oscillators, noise could for instance arise due to background vibrations or measurement errors.

In this paper we will investigate the effects of the additive noise on the qualitative behaviour of a piecewise-smooth map known as the *square root map* [14,15, 2,16,5]. The map can be derived as an approximation for solutions of a piecewise-smooth ordinary differential equation describing the dynamics of an *impact oscillator* near *grazing* (low-velocity) impacts [14,17] and it exhibits non-standard qualitative behaviour as a result of a discontinuity in its first derivative.

In smooth nonlinear systems the addition of noise has been shown to have the greatest effect on the outcome of the system in the neighbourhood of *bifurcation points* [18,11,12]. Bifurcation points are values of the system parameters that separate regions of parameter space where we observe topologically equivalent dynamics [7,8,10,25]. In nonsmooth dynamical systems, such as the square root map, we find certain types of bifurcations that do not occur in the smooth setting, known as *discontinuity induced bifurcations* [6,3]. We will focus on the effect of the introduction of noise near bifurcation points in the *period-adding cascade* of the square root map, a bifurcation structure which is unique to nonsmooth systems.

The remainder of this paper is organised as follows. In Section 2 we will describe the deterministic bifurcation structure of the square root map. Section 3 introduces noise to the square root map and presents our numerical observations of the effect of noise on the square root map in the neighbourhood of regions of multistability. In Section 4.1- 4.2 we examine relative levels of contraction and expansion in the deterministic square root map in order to explain the distinguishing features of the noise induced transitions between periodic behaviours observed in Section 3. We then examine how the steady state trajectory deviation distributions derived in [23] can interact with the deterministic features of the map to produce such transitions given appropriate noise amplitude in Section 4.3-4.4. A concluding discussion is presented in Section 5.

2 The Deterministic Square Root Map

2.1 The Map

We will first consider the one-dimensional square root map

$$x_{n+1} = S(x_n) = \begin{cases} S_L(x_n) = \mu + bx_n, & x_n < 0, \\ S_R(x_n) = \mu - a\sqrt{x_n}, & x_n \geq 0, \end{cases} \tag{1}$$

where $a > 0$, $0 < b < 1$, $S_L(x)$ is the linear part of the map applied on the left-hand side, and $S_R(x)$ is the square root part applied on the right. In this paper we will assume that the parameter b is such that $0 < b < \frac{1}{4}$. For values of b in this range the deterministic square root map undergoes a period-adding cascade with intervals of multistability as the bifurcation parameter μ is decreased [15]. We will discuss the deterministic structures of the square root map in this case more detail in Section 2.3.

2.2 Symbolic Dynamics

Here we will be interested in the qualitative behaviour of the map (1), i.e. whether an iterate is on the left-hand side of the map or on the right-hand side of the map, than the exact numerical value of each iterate. As a result we will describe the dynamics of the square root map through the use of *symbolic sequences*. Any orbit $\{x_n\}$ may be assigned a symbolic sequence $\{X_n\}$ comprised of the letters L and R, where

$$X_n = \begin{cases} L, \ x_n < 0, \\ R, \ x_n \geq 0. \end{cases} \tag{2}$$

Therefore, an L denotes an iterate on the left, while an R denotes an iterate on the right. Using symbolic sequences we will describe deterministic N-periodic orbits by their code $(R^{n_1}L^{n_2}\dots R^{n_{m-1}}L^{n_m})^\infty$, where $n_i \in \mathbb{N}$ and $\sum n_i = N$. On the other hand, an orbit with a corresponding symbolic sequence $(R^{n_1}L^{n_2}\dots R^{n_{m-1}}L^{n_m})^r$, where r is finite, will be described as undergoing
$R^{n_1}L^{n_2}\dots R^{n_{m-1}}L^{n_m}$ behaviour or dynamics for those rN iterates.

2.3 Bifurcations and Deterministic Structures

For $\mu < 0$ the map (1) has a globally stable fixed point. In the case where $\mu > 0$ Nordmark and other authors [14,15,3,16] have shown that:

1. If $0 < b < \frac{1}{4}$ there is a period-adding cascade of stable periodic orbits. That is, there are values of $\mu > 0$ for which a stable periodic orbit of period m with code $(RL^{m-1})^\infty$ exists for each $m = 2, 3, \dots$ with $m \to \infty$ as $\mu \to 0$. Moreover adjacent periodic overlap, i.e. there are values of $\mu > 0$ such that there are two stable periodic orbits, one with period m and code $(RL^{m-1})^\infty$ and the other with period $m+1$ and code $(RL^m)^\infty$. These are the only possible attractors except at bifurcation points.
2. If $\frac{1}{4} < b < \frac{2}{3}$ there is a period-adding cascade of stable periodic orbits such that stable periodic orbits of period m with code $(RL^{m-1})^\infty$ exist for each $m = 2, 3, \dots$. However, between period-m and period-$m+1$ windows we now see chaotic attractors.
3. If $\frac{2}{3} < b < 1$ as μ decreases towards zero there are a finite number of period-addings followed by a chaotic attractor on an interval of μ values that extends to $\mu = 0$.

We will focus on the first case where there is a period-adding cascade of stable periodic attractors with overlaps between adjacent periodic windows where we observe multistability. A bifurcation diagram for this case is shown in Figure 1. In the deterministic system (1) orbits of period m of the form $(RL^{m-1})^\infty$ exist as attractors over the range in the parameter μ given by

$$\mu_m^s < \mu < \mu_m^e, \tag{3}$$

where

$$\mu_m^s = \frac{1-b}{1-b^m}\left(\frac{a}{b}\right)^2\left(\frac{3}{4}\right)b^{2m} \tag{4}$$

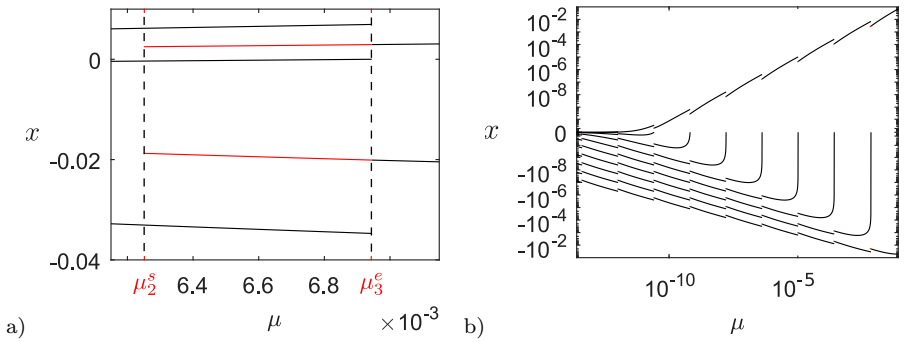

Fig. 1 Bifurcation diagrams for the deterministic square root map, S, with $a = 0.5$, $b = 0.2$. The threshold μ values for stability and existence are given by (4) and (5) while the iterates of the periodic orbits are given by (8) and (9). a) The coexistence of attractors $(RL)^\infty$ and $(RLL)^\infty$ for μ about the interval (μ_2^s, μ_3^e). The period-2 $(RL)^\infty$ orbit is coloured red on the interval of multistability. b) The period adding cascade of attractors $(RL^m)^\infty$ for $m \in \{1, \ldots, 10\}$. On the intervals of μ where $(RL^{m-1})^\infty$ and $(RL^m)^\infty$ coexist as attractors the iterates of $(RL^{m-1})^\infty$ are marked in red. A symmetric logarithmic transformation [24] has been applied to the x-axis in order to clearly show the structure of the period adding cascade.

is the threshold value for the stability of the period-m orbit and

$$\mu_m^e = \left[\frac{1-b}{1-b^{m-1}} a b^{m-2}\right]^2 \tag{5}$$

is the threshold value for its existence. We also have that

$$\mu_m^e > \mu_{m-1}^s > \mu_{m+1}^e > \mu_m^s \tag{6}$$

holds for $b < \frac{1}{4}$. This implies that if $\mu \in (\mu_{m-1}^s, \mu_m^e)$ then the stable periodic orbits $(RL^{m-2})^\infty$ and $(RL^{m-1})^\infty$ coexist. On the other hand, if $\mu \in (\mu_{m+1}^e, \mu_{m-1}^s)$ then a stable periodic orbit $(RL^{m-1})^\infty$ exists and is the only attractor. If $\mu \in (\mu_m^s, \mu_{m+1}^e)$ the pattern of coexistence starts again. We can see this period-adding behaviour and repeating pattern of coexistence clearly in the bifurcation diagram shown in Figure 1b) for orbits of period 2 to 11. In Figure 1a) we see an example of the coexistence of stable periodic orbits with codes $(RL)^\infty$ and $(RLL)^\infty$ on the interval (μ_2^s, μ_3^e). We will refer to the intervals, (μ_m^s, μ_{m+1}^e) on which stable periodic orbits $(RL^{m-1})^\infty$ and $(RL^m)^\infty$ coexist as *coexistence intervals* or *intervals of multistability*.

If R_m and $L_m^1, L_m^2, \ldots L_m^{m-1}$ are, respectively, the right iterate and left iterates of the deterministic period m orbit $(RL^{m-1})^\infty$ of S (see (1)) then using the fact that

$$S_L^{m-1}\left(S_R(R_m)\right) = R_m, \tag{7}$$

where S_L is the linear part (left-hand side) of the square root map and S_R is the the square root part (right-hand side), we find that

$$R_m = \left(\frac{1}{2}\left(-ab^{m-1} + \sqrt{(ab^{m-1})^2 + 4\sum_{i=0}^{m-1} b^i \mu}\right)\right)^2. \tag{8}$$

Hence we have that

$$L_m^1 = \mu - a\sqrt{R_m} \quad \text{and} \quad L_m^i = \mu + bL_m^{i-1} \tag{9}$$

for $i \in \{2, 3, \ldots, m-1\}$.

3 The Addition of Noise

3.1 The Square Root Map With Noise

We wish to examine the effect of uncertainty and noise on the square root map (1). In particular we are interested in the effect of noise on the period-adding cascade close to intervals of multistability, as discussed in Section 2.3.

Simpson and Kuske [20] show in a careful analysis that noise in impacting systems manifests itself in the corresponding two-dimensional square root map in several different ways, including coloured parametric noise. This is especially the case where there is coloured noise in the impacting dynamics of the full system. Hogan, Simpson and Kuske [19] show that the square root map in two dimensions with additive Gaussian white noise arises when the source of uncertainty in the full system is practically independent of the state of the system.

In this paper we consider small amplitude, additive, Gaussian white noise. However, our investigations indicate similar results for both additive and parametric noise of various distributions although we will not consider these noise formulations here. The square root map with additive Gaussian white noise that we consider is

$$\begin{aligned} x_{n+1} &= S_a(x_n) = \begin{cases} \mu + bx_n + \xi_n, & x_n < 0, \\ \mu - a\sqrt{x_n} + \xi_n, & x_n \geq 0, \end{cases} \\ \xi_n &\overset{\text{iid}}{\sim} N(0, \Delta^2), \end{aligned} \tag{10}$$

where ξ_n are identically distributed independent normal random variables with mean 0 and standard deviation Δ.

3.2 Numerical Observations

The effect of noise on the dynamics of a system with multiple coexisting attractors has long been of interest [22, 21, 9]. In this article we focus on phase-space sensitivity for values of the bifurcation parameter μ close to intervals where period-m and period-$(m+1)$ attractors coexist (6), but actually outside the interval itself. Investigating the effect of noise close to regions of multistability and the potential for such noise to attenuate the effect of bifurcation points has been done for the Duffing oscillator in [13]. Our numerical results indicate that a similar phenomenon occurs here in the square root map.

First, examining the neighbourhood of the coexistence interval (μ_2^s, μ_3^e) as a whole, in Figure 2 we plot numerically computed bifurcation diagrams for the square root map with additive Gaussian white noise (10) of varying amplitude. The corresponding analytic bifurcation diagram for the deterministic square root map (1) is shown in Figure 1a). For low noise amplitude we see both a reduction in the effective value of μ_3^e the threshold for the existence of the period-3 orbit and an increase in the effective value of μ_2^s the threshold for the stability of the period-2 orbit. This results in an effective shortening of the interval of multistability at

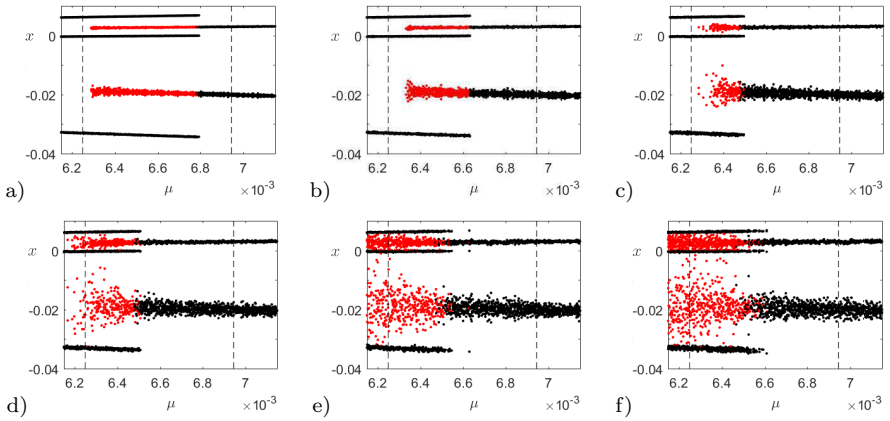

Fig. 2 Bifurcation diagrams for the square root map with additive Gaussian white noise (10), with increasing levels of noise amplitude, Δ = a) 2×10^{-5}, b) 4×10^{-5}, c) 6×10^{-5}, d) 8×10^{-5}, e) 1×10^{-4}, f) 1.2×10^{-4}, for μ in a neighbourhood of the coexistence interval (μ_2^s, μ_3^e). The deterministic values of μ_2^s and μ_3^e are indicated by dashed lines. Where the two periodic behaviours coexist the iterates of the behaviour with lower period are marked in red. For the corresponding deterministic bifurcation diagram refer to Figure 1a).

both end points compared to the deterministic system (see Figure 1a)). However, beyond some threshold further increases in noise amplitude appear to lead to an effective increase in the length of the coexistence interval. We see a weak return of RLL behaviour for higher values of μ but the effective value remains below the deterministic value of μ_3^s. On the other hand, RL behaviour appears to return for all values of $\mu > \mu_2^s$ and potentially extends into the region $\mu < \mu_2^s$. In this paper we are particularly interested in investigating the apparent presence of period-2 behaviour in a region where it is unstable in the corresponding deterministic system.

The bifurcation diagrams shown in Figure 2 leads us to believe that for fixed μ close to μ_2^s with increasing noise amplitude we first see a decrease in the probability of being in RL behaviour to some minimum followed by an increase in this probability as μ increases further. Looking at both the proportion of points in RL behaviour at a certain point in time and the proportion of time spent in RL behaviour over a long time period we have confirmed these relationships between noise amplitude and behaviour for additive noise. In particular, Figure 3 shows the relationship between the noise amplitude Δ and the proportion of time spent in RL behaviour, RLL behaviour and in transition between the two behaviours over 5,000 iterates, discounting 195,000 transients, for additive white noise where $\mu < \mu_2^s$. The bar chart shows the proportion of iterates spent by 1,000 orbits with linearly spaced initial conditions in each of the three types of behaviour. We see that, as expected, the deterministic system ($\Delta = 0$) exhibits only RLL behaviour once transients are discounted. This is also the case for the lowest noise amplitudes investigated. However, once the amplitude has been increased beyond some threshold Δ^*, we see that the addition of noise appears to induce some level of multistability, where both RL and RLL behaviours are present. This phenomenon could be considered to be a *phenomelogical bifurcation* or *p-bifurcation* [1].

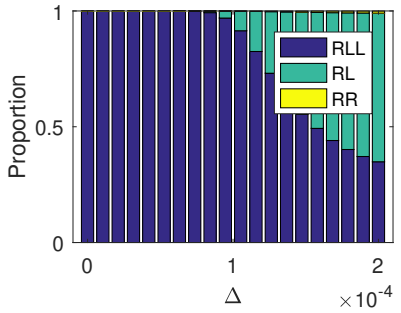

Fig. 3 Bar chart showing the changing proportion of time spent in RL & RLL behaviour and transition (RR) for increasing amplitude of additive noise, Δ, where $a = 0.5$ and $b = 0.2$ and $\mu = 0.00623 < \mu_2^s = 0.00625$. We plot the different relationships observed, considering dynamics over 5,000 iterates for 1,000 different orbits with linearly spaced initial conditions on the interval $[-0.04, 0.01]$ neglecting 195,000 transients.

A p-bifurcation refers to a qualitative change in the topology of the stationary distribution of a dynamical system. Here we see that noise above the threshold amplitude causes the stationary monostable distribution of the square root map to become multistable.

3.3 The Evolution of Deviations

In order to more formally understand how the addition of noise affects the qualitative behaviour of the square root map we will use an approximation for the distribution of trajectory deviations resulting from the addition of noise to the system derived in [23]. In particular we are interested in how these deviations can be related to the persistence of unstable periodic behaviour. Using an approach involving linearisation the authors of [19] have derived approximate invariant Gaussian densities associated with periodic attractors of the square root map in two dimensions.

We consider two trajectories, $\{x_k\}$ and $\{z_k\}$, with identical initial conditions $x_0 = z_0 = R_{m+1}$, i.e. two trajectories with initial conditions equal to the right iterate of the deterministic $(RL^m)^\infty$ orbit of the system. We then iterate forward using the square root map with additive noise (10) in the case of x_0, letting $x_{k+1} = S_a(x_k)$, and the deterministic square root map (1) in the case of z_0, letting $z_{k+1} = S(z_k)$. The deviation due to noise in the trajectory $\{x_k\}$ is then given by the difference $\{\epsilon_k\} = \{x_k - z_k\}$. From (1) and (10) we have that, provided the deviations are not so large as to push $\{z_k\}$ out of RL^m behaviour, the error terms ϵ_k are given by

$$\epsilon_k = x_k - z_k = \begin{cases} a\psi_{k-1} + \xi_{k-1}, & k \bmod (m+1) = 1, \\ b\epsilon_{k-1} + \xi_{k-1}, & \text{otherwise}, \end{cases} \tag{11}$$

with $\epsilon_0 = 0$ and $\psi_{k-1} = \sqrt{R_{m+1}} - \sqrt{R_{m+1} + \epsilon_{k-1}}$. Referring to [23] we have that ϵ_k is distributed approximately normal for all k with distribution $N(0, \sigma_{\epsilon_k}^2)$. Here

the variances are given by

$$\sigma^2_{\epsilon_k} = \begin{cases} \dfrac{a^2\sigma^2_{\epsilon_{k-1}}}{4R_{m+1}} + \Delta^2, \; k \bmod (m+1) = 1, \\ b^2\sigma^2_{\epsilon_{k-1}} + \Delta^2, \;\; \text{otherwise.} \end{cases} \tag{12}$$

Working $\bmod(m+1)$ we can write (12) as a system of $m+1$ difference equations

$$\sigma^2_{\epsilon_{(n+1)(m+1)+k}} = f_k(\sigma^2_{\epsilon_{n(m+1)+k}}) \tag{13}$$

with initial conditions given by $\sigma^2_{\epsilon_k}$ for $1 \leq k \leq m+1$. The map f_k has a fixed point $\hat{\sigma}^2_{k,(m+1)}$ for each of the $m+1$ difference equations such that

$$\hat{\sigma}^2_{k,(m+1)} = \Delta^2 \left(\frac{a^2 \displaystyle\sum_{i=k}^{m} b^{2(i-1)} + 4R_{m+1} \sum_{i=0}^{k-1} b^{2i}}{4R_{m+1} - (ab^m)^2} \right). \tag{14}$$

We require $\hat{\sigma}^2_{k,(m+1)} > 0$ and so (8) and (14) imply that

$$4R_{m+1} = \left(-ab^m + \sqrt{(ab^m)^2 + 4\sum_{i=0}^{m} b^i \mu} \right)^2 > (ab^m)^2, \tag{15}$$

which gives that

$$\mu > \frac{3}{4}\left(\frac{1-b}{1-b^{m+1}}\right)(ab^m)^2 = \mu^s_{m+1} \tag{16}$$

and so the fixed points given in (14) exist for values of μ in the interval of stability for the deterministic $(RL^m)^\infty$ orbit, $(\mu^s_{m+1}, \mu^e_{m+1})$, with $\hat{\sigma}^2_{k,(m+1)} \to \infty$ as $\mu \to \mu^{s^+}_{m+1}$ since the numerator $\to a^2\Delta^2 \left(\displaystyle\sum_{i=k-1}^{m+k-1} b^{2i} \right)$ as $\mu \to \mu^{s^+}_{m+1}$. On the other hand, $\hat{\sigma}^2_{k,(m+1)} \to c$ where $c > 0$ as $\mu \to \mu^{e^-}_{m+1}$.

The difference equations (13) converge for

$$\mu \in \left(-4a^{-2} \sum_{i=0}^{m} b^{i-2m}, 12a^{-2} \sum_{i=0}^{m} b^{i-2m} \right) := A_\mu. \tag{17}$$

Now, since $0 < b < \frac{1}{4}$ and $0 < a < 1$ we have that

$$(\mu^s_{m+1}, \mu^e_{m+1}) \subset \left[0, 12 \sum_{i=m}^{2m} 4^i \right] \subset A_\mu \tag{18}$$

and so (13) converges for all relevant values of the bifurcation parameter μ and all k.

Taking $m = 2$ as an example and examining the case of deviations on the last left iterate L^2_3 of the deterministic period-3 orbit for $\mu < \mu^s_2$, we can see that the analysis in Section 3.3 agrees well with our numerical results. Taking one million

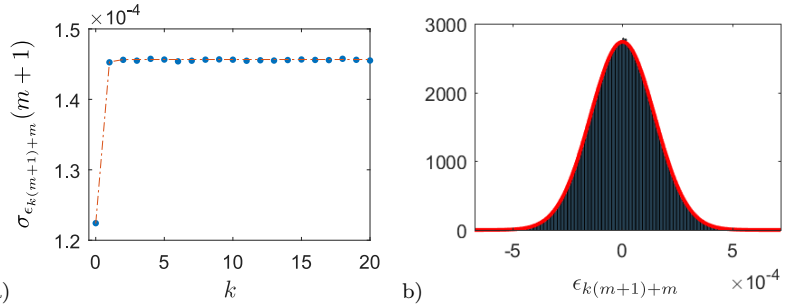

Fig. 4 a) The evolution of the standard deviations of the normal fits of the distributions of the deviations ϵ_m and $\epsilon_{k(m+1)+m}$ such that $\epsilon_{(k-1)(m+1)+m} < -L_{m+1}^m$ for $1 \leq k \leq 20$, fitted using MATLAB®'s `fitdist` function, (blue circles) compared to our semi-analytic prediction given by (13) (red dashed line). b) The histogram and normal fits of the distributions (red curve) of the deviations $\epsilon_{7(m+1)+m}$ such that $\epsilon_{(k-1)(m+1)+m} < -L_{m+1}^m$ for $1 \leq k \leq 7$.

orbits with initial condition $x_0 = R_3$ we examine the distribution of the deviations $\epsilon_{n(3)-1}$ for $n = 1, 2, \ldots, 100$, such that $\epsilon_{k(3)-1} < -L_3^2$ for $k < n$. In Figure 4a) we show that the fitted normal distributions, (fit using the MATLAB® `fitdist` function) of these deviations appear to have an approximately zero mean with standard deviation converging quickly to some limit, $\bar{\sigma}$ as $n \to \infty$. We see that the standard deviations of these fitted distributions closely mirror the approximate standard deviations predicted by our analysis (13), in particular the standard deviations do indeed appear to converge to the value of $\hat{\sigma}_{2,3}$ given by (14). In Figure 4b) we compare an example of these fitted normal distributions to the histogram of the observed numerical deviations and find that the fitted distributions are indeed good fits for the actual distributions. We can therefore use the approximate deviation distributions derived in Section 3.3 to better understand the noise induced transitions observed in the square root map.

4 The Persistence of Unstable Behaviour Due to Noise

Let us now return to examine in more detail the potential for repeated intervals of persistent RL^{m-1} dynamics in a noisy system of sufficiently high noise amplitude with $\mu < \mu_m^s$, as observed in Figure 2 in the $m = 2$ case. A related phenomenon for a system with $\mu > \mu_m^s$ is that the proportion of time spent by the system in RL^{m-1} behaviour falls to almost zero as noise amplitude increases to some threshold value, effectively destroying the attractor. However, for noise amplitudes above this threshold RL^{m-1} behaviour returns [23].

In order to explain the persistence of unstable periodic behaviour in the stochastic square root map (10), in Section 4.1 we will first look for qualitative similarities in observed noise-induced transitions from stable to unstable periodic behaviour. These transitions are essential in inducing multistability in regions in which only one stable periodic attractor exists in the deterministic system (1). Without them the system would simply remain in a noisy version of the stable periodic orbit. We will then explain why the observed similarities between noise-induced transitions exist by referring to features of the deterministic square root map (1) in Section

4.2. By referring to Section 3.3 in Section 4.3 we will show additive Gaussian white noise can induce transitions of the form observed and in Section 4.4 we will present examples of such transitions observed in numerical simulations.

4.1 The Transition

In the numerical simulations we have found that noise-induced transitions between RLL and RL behaviour display certain similarities. In particular, we have observed that the transitions tend to take the following symbolic form

$$RLLRLL\ldots RLL\underline{RLLRLRRL}RL\ldots RLRL. \tag{19}$$

The significant feature of the symbolic representation of the transition (19) is the repeated R corresponding to repeated iteration by S_R on the right-hand side of the square root map (1).

In general we see that the features of this transition are repeated as we look at transitions from RL^m behaviour to RL^{m-1} behaviour for increasing m. In particular we observe transitions of the form

$$RL^mRL^m\ldots\underline{RL^mRL^{m-1}RL^{k-2}RL^{m-1}RL^{m-1}}\ldots \\ \ldots RL^{m-1}RL^{m-1} \tag{20}$$

for μ in a neighbourhood of μ_m^s such that $\mu<\mu_m^s$ and $k\in\{2,3,\ldots,m\}$. The most significant feature of transitions of the form given in (20) is the sequence $RL^{k-2}R$ for $k\in\{2,3,\ldots,m\}$, again corresponding to iterations on the right-hand side of the map being repeated more quickly than is usual for a settled system with $\mu<\mu_m^s$.

4.2 Contraction and Expansion

In order to understand the effect of noise on the square root map, and the importance of the form of the transition characterised by (20), we will look at the sets associated with the occurrence of this symbolic sequence in the deterministic dynamical system (1). Let $A_{X_1X_2\ldots X_m}$ denote the set of values $x_1\in\mathbb{R}$ such that the sequence $x_1,x_2,\ldots,x_m$, generated under iteration by (1) has the symbolic representation $X_1,X_2,\ldots,X_m$. For example, the set A_{LL} is the set of values to the left of zero, i.e. less than zero, that remain on the left after a single iteration. We can construct A_{LL} as

$$\begin{aligned} A_{LL} &\coloneqq \{x\in(-\infty,0):S(x)<0\} \\ &= \{x\in(-\infty,0):\mu+bx<0\}=\left(-\infty,-\frac{\mu}{b}\right) \end{aligned} \tag{21}$$

and similarly we find

$$\begin{aligned} A_{LR} &\coloneqq \left(-\frac{\mu}{b},0\right), \\ A_{RR} &\coloneqq \left(0,\left(\frac{\mu}{a}\right)^2\right), \\ A_{RL} &\coloneqq \left(\left(\frac{\mu}{a}\right)^2,\infty\right). \end{aligned} \tag{22}$$

Noting that

$$A_{X_0X_1\ldots X_m} = \{x \lesseqgtr 0 : S(x) \in A_{X_1\ldots X_m}\} \tag{23}$$

for $X_0 = L$ or R respectively, we can find the set $A_{\{X_i\}}$ associated with any symbolic sequence $\{X_i\}$ of finite length iteratively.

The sets $A_{X_1X_2\ldots X_m}$ become small very quickly as the length of the sequence $X_1, X_2, \ldots, X_m$ increases. In fact the sets associated with the longest symbolic sequences lie outside $[\mu - a\sqrt{\mu}, \mu]$, the settled range of the map. The small sizes of these intervals, or their location outside the map's settled range, lead us to believe that the noise-induced transition mechanism observed in simulations is not likely based entirely on being pushed into one of the sets associated with a longer sequence, which were derived based on the deterministic mapping. As a result we wish to investigate the properties of the sets associated with shorter sequences.

We have noted previously that the most significant feature of the transition given in (20) is the sequence $RL^{k-2}R$ corresponding to iterations on the right being repeated more quickly than is usual for a settled system. As a result we would like to see what the images of $A_{RL^{k-2}R}$ look like under iteration by S. The nature of these images may give us a better understanding of why close-together iterations on the right-hand side of the map lead to a transition to RL^{m-1} behaviour. First we recall from (22) that

$$A_{RR} = \left(0, \left(\frac{\mu}{a}\right)^2\right) \tag{24}$$

and note that

$$A_{RL^{k-2}R} = \left(\left(\frac{\mu}{a}\sum_{i=0}^{k-3} b^{-i}\right)^2, \left(\frac{\mu}{a}\sum_{i=0}^{k-2} b^{-i}\right)^2\right) \tag{25}$$

for $k \in \{3, 4, \ldots, m\}$. These sets are located just to the right of zero and their relative sizes are shown in Figure 5a. As a result, a small positive deviation due to low amplitude noise could push settled RL^m dynamics (a slightly blurred version of the stable deterministic $(RL^m)^\infty$ orbit) into one of these sets. This is because L^m_{m+1}, the m^{th} left iterate of that stable orbit, is very close to zero.

Let us now look at the images of these sets under iteration by S. We have that the $(k-1)^{\text{th}}$ and k^{th} images of $A_{RL^{k-2}R}$ under iteration by the square root map (1) are given by

$$\begin{aligned} S^{k-1}(A_{RL^{k-2}R}) &= (0, \mu) \quad \text{and} \\ S^{k}(A_{RL^{k-2}R}) &= (\mu - a\sqrt{\mu}, \mu)\,. \end{aligned} \tag{26}$$

Any trajectory $\{x_0, x_1, x_2, \ldots\}$ iterated under the deterministic square root map (1) with initial condition $x_0 < 0$ will be increasing for the first j iterations, where $j \in \mathbb{N}$ is the minimum such that $x_j > 0$. This is as a result of the fact that $\mu > 0$ and $0 < b < \frac{1}{4}$. Furthermore since $x_{j-1} < 0$ we will have that $x_j \in (0, \mu)$. Any trajectory with initial condition $x_0 \in ((\mu/a)^2, \infty) = A_{RL}$ will be such that $x_1 < 0$, while (26) gives that the image of $(0, (\mu/a)^2) = A_{RR}$ is $(0, \mu)$ and so any trajectory with initial condition $x_0 < 0$ will also eventually enter the set $(0, \mu)$. Finally the image of the set $(0, \mu)$ under a single iteration of the square root map $S((0, \mu)) = (\mu - a\sqrt{\mu}, \mu)$. This means that for any trajectory iterated under the

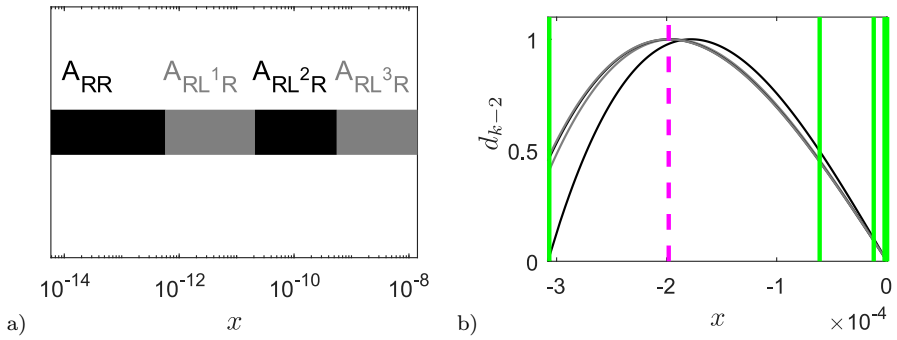

Fig. 5 a) Graphical representation on a log scale of the sets $A_{RL^{k-2}R}$ for $k \in \{2,3,\ldots,5\}$ for $\mu = 0.99\mu_5^s$. b) The distributions, $(x_{k-2}(s), d_{k-2}(s))$, of the images of the sets $A_{RL^{k-2}R}$ under g_{k-2} for $k \in \{2,\ldots,5\}$ where $\mu = 0.99\mu_5^s$. L_5^1, the first left iterate of the unstable $(RL^4)^\infty$ orbit, is indicated by the dashed magenta line. The 6 iterates of the stable $(RL^5)^\infty$ obit are indicated by solid green lines.

square root map $\exists N \in \mathbb{N}$ such that $\forall n > N$ we have $x_n \in [\mu - a\sqrt{\mu}, \mu]$ and so this gives us no more information as to why repeated iterations on the right tend to result in a transition to RL^{m-1} behaviour.

Instead we will examine the relative levels of expansion and contraction experienced by elements of $A_{RL^{k-2}R}$ under iteration by S. We show that for μ in a neighbourhood of μ_m^s, the first iterate on the left of the unstable deterministic orbit $(RL^{m-1})^\infty$ is 'close' to x_t^{k-2} where x_t^{k-2} is the mode of the distribution of the k^{th} image of the set $A_{RL^{k-2}R}$ for $k \in \{2,3,\ldots,m\}$.

For $x \in A_{RL^{k-2}R}$ we have that $x > 0$ and

$$\begin{aligned} S^k(x) &= S_R(S_L^{k-2}(S_R(x))) \\ &= \mu - a\sqrt{\mu\sum_{i=0}^{k-2} b^i - ab^{k-2}\sqrt{x}} := g_{k-2}(x). \end{aligned} \tag{27}$$

This gives that that

$$g'_{k-2}(x) = \frac{a^2 b^{k-2}}{4} \frac{1}{\sqrt{x}\sqrt{\mu\sum_{i=0}^{k-2} b^i - ab^{k-2}\sqrt{x}}}, \tag{28}$$

where the dash $'$ indicates differentiation with respect to x. We observe that $g'_{k-2}(x) \to \infty$ as $x \to 0^+$ and as $x \to \left(\left(\frac{\mu}{a}\sum_{i=0}^{k-2} b^{-i}\right)^2\right)^-$. This means that the level of expansion experienced by elements of the interval $A_{RL^{k-2}R}$ over the course of two close together iterations on the right tends to infinity as we approach the endpoints. On the other hand, the elements of $A_{RL^{k-2}R}$ that experience the least expansion over the course of two close together iterations on the right are the points about x_c^{k-2}, where x_c^{k-2} is such that the second derivative of g_{k-2} with respect to x, $g''_{k-2}(x_c^{k-2}) = 0$. As a result, the image of linearly spaced points in $A_{RL^{k-2}R}$ will

be concentrated about $g_{k-2}(x_c^{k-2}) = x_t^{k-2}$ with distribution $(x_{k-2}(s), d_{k-2}(s))$, where

$$x_{k-2}(s) = g_{k-2}(s) = \mu - a\sqrt{\mu\sum_{i=0}^{k-2} b^i - ab^{k-2}\sqrt{s}} \tag{29}$$

and

$$d_{k-2}(s) = \frac{1}{g'_{k-2}(s)} = \frac{4\sqrt{s}}{a^2b^{k-2}}\sqrt{\mu\sum_{i=0}^{k-2} b^i - ab^{k-2}\sqrt{s}}, \tag{30}$$

for $s \in A_{RL^{k-2}R}$. Calculating the second derivative of g_{k-2} we find that

$$g''_{k-2}(x) = \frac{a^2b^{k-2}}{16}\frac{3ab^{k-2}\sqrt{x} - 2\mu\sum_{i=0}^{k-2} b^i}{\left(x\left(\mu\sum_{i=0}^{k-2} b^i - ab^{k-2}\sqrt{x}\right)\right)^{\frac{3}{2}}}. \tag{31}$$

Now, x_c^{k-2} is given by finding the roots of (31) and thus

$$g''_{k-2}(x_c^{k-2}) = 0 \implies x_c^{k-2} = \frac{4}{9}\left(\frac{\mu}{a}\right)^2\left(\sum_{i=0}^{k-2} b^{-i}\right)^2, \tag{32}$$

which gives that

$$S(x_c^{k-2}) = \mu - a\sqrt{x_c^{k-2}} = \left(1 - \frac{2}{3}\sum_{i=0}^{k-2} b^{-i}\right)\mu \tag{33}$$

and

$$x_t^{k-2} = S^k(x_c^{k-2}) = g(x_c^{k-2}) = \mu - a\sqrt{\frac{\mu}{3}\sum_{i=0}^{k-2} b^i}. \tag{34}$$

The point x_t^{k-2}, around which the image of $A_{RL^{k-2}R}$ for $k \in \{2, \ldots, m\}$ is concentrated after undergoing two close together iterations on the right, is close to L_m^1, the first left iterate of the $(RL^{m-1})^\infty$ orbit of the deterministic system.

When μ is in the neighbourhood of μ_m^s points in $A_{RL^{k-2}R}$, where $2 \le k \le m$, undergo two iterations on the right-hand side of the map by S_R in the first $k \le m$ iterates. This corresponds to iterations on the right-hand side of the map being repeated more quickly than is usual for a settled system where it takes at least $m+1$ iterates to repeat iterations on the right. The distribution of the image of $A_{RL^{k-2}R}$ after k iterates, the first and last of which are by S_R, along with the high number of iterates required by orbits to enter RL^m behaviour for $x_0 \in A_{RL^{k-2}R}$, gives us a significant insight into why the sequence $RL^{k-2}R$ is such an important feature of the noise induced transition from RL^m to RL^{m-1} behaviour in the noisy version of the square root map.

To illustrate this, in Figure 5b) we plot the distributions $(x_{k-2}(s), d_{k-2}(s))$ given in (30), of the images of the sets $A_{RL^{k-2}R}$ after undergoing two close together iterations on the right for $m = 5$ and $k \in \{2, \ldots, 5\}$ where $\mu < \mu_5^s$. We observe that the modes of all four distributions are very close to the first left iterate of the

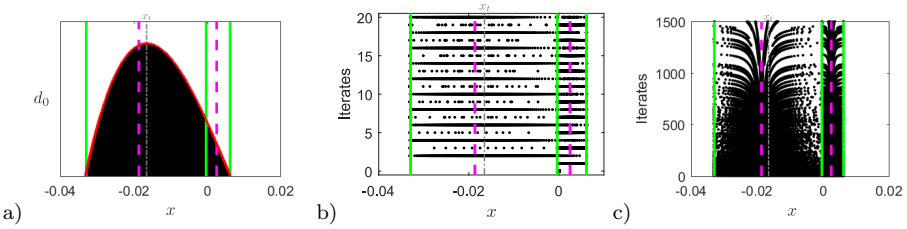

Fig. 6 a) Histogram showing the distribution of the image of 100,000 linearly spaced points in A_{RR} after two iterations, $S^2(A_{RR})$ along with $d_0(s)$ in red. b) and c) Iterates of 300 linearly spaced points in A_{RR} under the square root map S, 20 times and until divergence from RL behaviour respectively. In all three cases we have taken $\mu < \mu_2^s$. The iterates of the stable $(RLL)^\infty$ orbit of the system are marked in green, the iterates of the unstable $(RL)^\infty$ orbit of the system are marked in dashed magenta and x_t is marked in dash-dotted grey.

unstable $(RL^4)^\infty$ orbit, especially when compared to their distance to any of the iterates of the stable RL^5 orbit. As a result of this, any orbit that enters one of the sets $A_{RL^{k-2}}$ for $k \in \{2, 3, \ldots, 5\}$, when $\mu < \mu_5^s$, will take a long time to exit RL^4 behaviour and converge to $(RL^5)^\infty$, the only stable attractor in the system in that case. In general any noisy RL^m orbit pushed into one of the sets $A_{RL^{k-2}R}$ for $k \in \{2, 3, \ldots, m\}$ has the potential to transition into RL^{m-1} behaviour for a sustained period of time.

In order to illustrate this behaviour let us take the $m = 2$ case and examine the transition from RLL to RL behaviour as a example. We will consider values of $\mu < \mu_2^s$ in a small neighbourhood of μ_2^s where this orbit is unstable. In this case we have only one choice of k corresponding to close together iterations by S_R, $k = m = 2$, and so we are concerned only with the images of the set A_{RR}. After two iterations on the right the distribution of linearly spaced orbits in A_{RR}, given by (30) and shown in Figure 6a), is concentrated around x_t (34), close to L_2^1, the left iterate of the $(RL)^\infty$ orbit of the deterministic system. Orbits with initial conditions close to L_2^1 will take a significant number of iterates to leave RL behaviour and converge to the $(RLL)^\infty$ attractor for such values of μ. This is clearly illustrated by Figures 6b) and 6c). We examine 300 orbits with linearly spaced initial conditions in A_{RR}. We observe that, as a result of this distribution, a significant proportion of the orbits with initial conditions in A_{RR} do not exit RL behaviour until after a substantial number of iterations. Indeed, after 1500 iterates a proportion of the orbits are still in RL behaviour.

In general, the number of iterates required by orbits with different initial conditions to enter RLL behaviour for the first time for μ in a neighbourhood of μ_2^s has a very complicated structure. We have plotted this for the entire settled range of the map $[\mu - a\sqrt{\mu}, \mu]$, and in more detail, for the subset A_{RR} in Figure 7. This complicated structure is analagous to the *riddled* structure of the basins of attraction of the coexisting periodic attractors on intervals of multistability as discussed in [23].

We can now fully understand why a double R, corresponding to repeated iterations on the right, is such an important feature of the noise-induced transition from RLL to RL behaviour in the noisy version of the square root map (10). Our analysis suggests that trajectories entering A_{RR} could take a significant number of iterates to return to RLL behaviour due to the deterministic structures of the map.

We also can see that, as L_3^2, the second left iterate of the deterministic $(RLL)^\infty$ orbit is close to zero for μ in a neighbourhood of μ_2^s ($|L_3^2| \lll 1$), small deviations due to noise would be enough to push an orbit from RLL behaviour near the deterministic orbit into the set $A_{RR} = \left(0, (\mu/a)^2\right)$. The combination of these features means that noise has the potential to push trajectories from RLL behaviour into A_{RR} and as a result concentrate these trajectories around the unstable $(RL)^\infty$ orbit of the deterministic system where they have the potential to remain for a significant number of iterates.

4.3 Deviation Distributions Under Repeated Iteration on the Right

We can now combine our knowledge of the steady-state deviations of the period-$(m+1)$ orbit derived in Section 3.3, the expansion and contraction undergone during repeated iterations on the right-hand side of the square root map described in Section 4.2 and the complicated structure of the relationship between initial conditions and the number of iterates required to transition to the stable period-$(m+1)$ orbit in the deterministic map shown in Figure 7 to better understand the persistence of unstable periodic behaviour. Again, taking the $m = 2$ case as an example, we know from Section 4.2 that deviations $\epsilon_{n(3)-1}$ such that $-L_3^2 < \epsilon_{n(3)-1} < -L_3^2 + (\mu/a)^2$ will induce consecutive iterations on the right, symbolically RR.

We consider the steady-state distribution of $L_3^2 + \epsilon_{n(3)-1}$, i.e. the normal distribution with mean L_3^2 and standard deviation $\hat{\sigma}_{2,3}$. We then truncate this distribution to the interval $\left(0, (\mu/a)^2\right) = A_{RR}$ to find the distribution Tf which is shown in Figure 7b). Mapping this distribution under consecutive iterations on the right gives us the distribution $S_R^2(Tf)$, shown in Figure 7c). We see the mode of this distribution is close to the unstable left iterate of the RL orbit, and in a region where orbits will take a significant number of iterates to return to RLL behaviour. In fact, taking $\mu = 0.99\mu_2^s$ and $\Delta = 1.2 \times 10^{-4}$ we find that the expected number of iterates to return to period-3 behaviour for an orbit whose deviation has pushed the last left iterate on the right-hand side is given by

$$E(\text{Iterates to return} |\ \epsilon_{(n+1)(3)-1} \in (-L_3^2, -L_3^2 + (\mu/a)^2)) \approx 175, \tag{35}$$

with standard deviation

$$\sigma(\text{Iterates to return} |\ \epsilon_{(n+1)(3)-1} \in (-L_3^2, -L_3^2 + (\mu/a)^2)) \approx 255, \tag{36}$$

where we iterate forward using the deterministic square root map (1).

4.4 Examples

In Figure 8a) we show an example of a transition from RLL to RL behaviour of the form given in (19) along with the associated noisy signal. We focus on the the characteristics of the noisy signal $\xi_0, \xi_1, \ldots, \xi_7$ associated with the eight iterates $x_0, x_1, \ldots, x_7$ represented by the underlined portion of the symbolic sequence

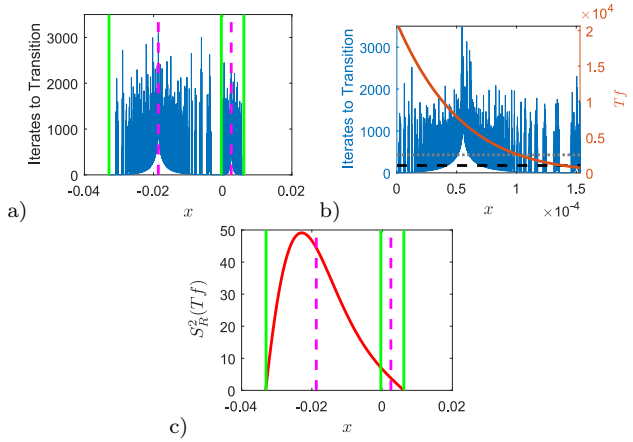

Fig. 7 a) The number of iterates required for orbits with a range of initial conditions to transition to RLL behaviour in the deterministic system where $\mu < \mu_2^s$. b) The steady-state distribution of the last left iterate of the RLL orbit truncated to A_{RR}, Tf, along with E(Iterates to return to period-3 behaviour) ≈ 175 marked in dashed black and E(Iterates to return to period-3 behaviour) plus one standard deviation ≈ 430 in dotted grey. c) The distribution of iterates with deviations $\epsilon_{n(3)-1}$ such that $-L_3^2 < \epsilon_{n(3)-1} < -L_3^2+(\mu/a)^2$ after undergoing repeated iterations on the right-hand side of the square root map. For the distributions in both b) and c) we have taken $\Delta = 1.2 \times 10^{-4}$.

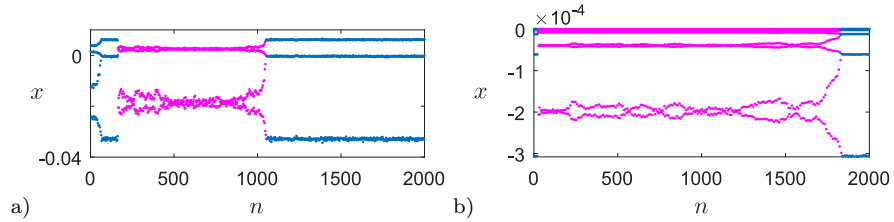

Fig. 8 a) An example of a noise-induced transition from settled RLL to persistent RL behaviour in the square root map with additive noise and $\mu < \mu_2^s$ and the associated noisy signal. Here $\Delta = 1.2 \times 10^{-4}$ and $\mu = 0.0062$. b) An example of a noise-induced transition from settled RL^5 to persistent RL^4 behaviour in the square root map with additive noise and $\mu < \mu_5^s$. Here $k = 4$.

(19) and note that none of the individual noise terms have an exceptionally large magnitude. Instead in Figure 9 we see that the transition is triggered by the accumulated deviation term $\epsilon_5 > -L_3^2$, which pushes the trajectory into the set A_{RR} resulting in repeated iterations on the right.

In Figure 9b) we also see that the orbit in the noisy system remains in RL behaviour for a far longer period of time than the equivalent orbit with the same initial condition x_7 in the deterministic system. This means that noise can play a role in maintaining RL behaviour in systems with $\mu < \mu_2^s$, in essence "stabilising" an orbit which is unstable in the associated deterministic system. We have not yet been able to find any precise characteristics of a noisy signal that is likely to result in such "stabilisation" however it is something we intend to look at in the future.

In Figure 8b) we show an example of a transition of the form given in (20), for $m = 5$ and $k = 4$. From results of experimental simulation of noisy square root

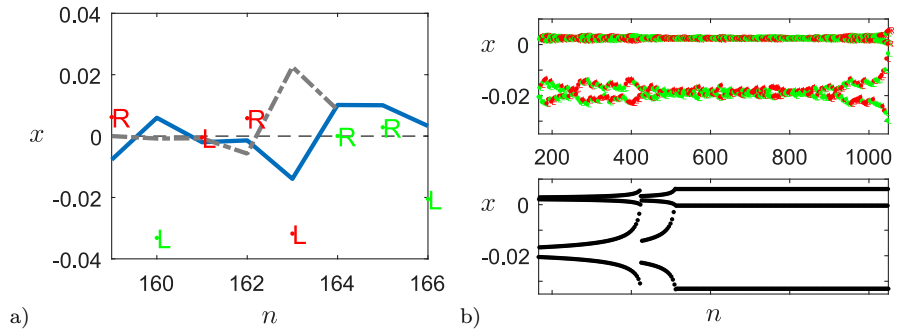

Fig. 9 a) The iterates $x_0, \ldots, x_7$ associated with the eight underlined terms in the symbolic sequence (19) in the case of the transition shown in Figure 8a). We also show their associated noise terms $\xi_0, \ldots \xi_7$ in blue and the associated deviation terms of the first 6 iterates $\epsilon_0, \ldots, \epsilon_5$ in dash-dotted grey (not to scale). b) A close-up look at the persistent noise induced RL behaviour shown in in Figure 8a) and the associated deterministic square root map dynamics with initial condition given by x_7, where the iterates $x_0, \ldots, x_7$ are the iterates associated with the eight underlined terms in the symbolic sequence (19).

maps with μ in a neighbourhood of μ_m^s such that $\mu < \mu_m^s$ for different values of m it appears that transitions with certain k values occur more frequently and other k values are associated with the "best" transitions. For example, in the $m = 5$ case many of the "best" transitions were associated with symbolic sequences of the form given in (20) with $k = 4$. We hypothesise that this is related to both the size and the ordering of the sets $A_{RL^{k-2}R}$ to the right of zero. For example A_{RR} becomes vanishingly small as m increases and so orbits are less likely to enter this set. On the other hand, when $k = m$ the set $A_{RL^{m-2}R}$ is the largest of these intervals, but is also located the furthest to the right and so requires a large deviation for orbits to enter. If an orbit does enter this set it is likely to be near to the left endpoint and so its image after two close together iterations on the right-hand side of the square root map is not likely to be too close to L_m^1, resulting in a "weak" transition. As a result, we believe that "strong" transitions will generally be associated with k values that are greater than 2 and less than m. The sets $A_{RL^{m-2}R}$ for $k \in \{3, \ldots, m-1\}$ are larger than A_{RR} but closer to the left than $A_{RL^{m-2}R}$ and so noisy orbits are more likely to have iterates landing near the centre of these sets, whose images after two close together iterations on the right will be near to L_m^1 and thus result in a strong transition.

5 Discussion

This paper is concerned with the effects of the introduction of small amplitude additive Gaussian white noise on the dynamics of the square root map (1). This noise formulation (10) was shown in [19] to be consistent with state-independent noise in piecewise-smooth ordinary differential equations describing an impact oscillator with low-velocity impacts. Our investigations show that introducing noise of this type to the one-dimensional square root map has the potential to induce significant changes in the qualitative behaviour of the system.

In particular, we have investigated the effect of noise on the period-adding cascade of the map, which exists for $0 < b < \frac{1}{4}$ in the deterministic system. This

period-adding cascade is such that there are values of the bifurcation parameter $\mu > 0$ for which a stable periodic orbit of period m exists for each $m = 2, 3, \ldots$, and also such that there are two stable periodic orbits, one period-$(m+1)$ orbit and one period-m orbit.

In Section 3.2 (see Figures 2-3) we have shown numerical evidence for the persistence of unstable periodic behaviour in the neighbourhood of intervals of multistability due to the addition of noise to the system. In other words, noise of sufficient amplitude effectively induces multistability in these regions in a p-bifurcation. In such regions we identified features of noise-induced transitions from stable to unstable periodic behaviour, including the transition's symbolic representation which is given by (20). In Section4.1-4.2 we have highlighted that the defining feature of these transitions is the presence of two iterations on the right-hand side of the map, separated by a small number of iterations on the left, i.e. less than the number of iterates on the left of the unstable periodic orbit. Our investigations revealed that trajectories that are iterated in the order given by (20) become concentrated around the unstable periodic orbit due to relative levels of expansion and contraction during iteration. Such trajectories are likely to take a significant number of iterates to return to the stable periodic behaviour (see Figure 6).

Finally, we show in Section 4.3-4.4 that noise-induced transitions from stable to unstable periodic behaviour can be understood by examining how estimates of the steady-state distributions of deviations due to noise derived in [23] interact with the deterministic structures of the map. We also present examples of such transitions, from period-3 to period-2 behaviour and from period-6 to period-5 behaviour, in numerical simulations in Figures 8-9.

In addition to the investigation required to more formally understand what features of a noisy signal are require to drive "strong" transitions and to "stabilise" unstable behaviour once a noise-induced transition occurs, several problems remain for future work. In particular, it remains to be shown how these results can be extended to the case of the two-dimensional square root map derived as an approximation for the full system describing an impact oscillator near grazing and indeed to the full ODE system itself.

Acknowledgements We are grateful for the hospitality of CRM, Barcelona, where this work was started and to Paul Glendinning for his helpful input in the early stages.

Conflicts The authors declare that they have no conflict of interest.

References

1. Arnold, L., Boxler, P.: Stochastic bifurcation: instructive examples in dimension one. In: Diffusion Processes and Related Problems in Analysis, Volume II, pp. 241–255. Springer (1992)
2. Avrutin, V., Dutta, P.S., Schanz, M., Banerjee, S.: Influence of a square-root singularity on the behaviour of piecewise smooth maps. Nonlinearity **23**(2), 445 (2010)
3. Bernardo, M., Budd, C., Champneys, A.R., Kowalczyk, P.: Piecewise-smooth dynamical systems: theory and applications, vol. 163. Springer Science & Business Media (2008)
4. Bishop, S.: Impact oscillators. Philosophical Transactions of the Royal Society of London A: Mathematical, Physical and Engineering Sciences **347**(1683), 347–351 (1994)

5. Chin, W., Ott, E., Nusse, H.E., Grebogi, C.: Grazing bifurcations in impact oscillators. Physical Review E **50**(6), 4427 (1994)
6. Di Bernardo, M., Budd, C.J., Champneys, A.R., Kowalczyk, P., Nordmark, A.B., Tost, G.O., Piiroinen, P.T.: Bifurcations in nonsmooth dynamical systems. SIAM review **50**(4), 629–701 (2008)
7. Guckenheimer, J.: On the bifurcation of maps of the interval. Inventiones mathematicae **39**(2), 165–178 (1977)
8. Guckenheimer, J., Holmes, P.J.: Nonlinear oscillations, dynamical systems, and bifurcations of vector fields, vol. 42. Springer Science & Business Media (2013)
9. Kraut, S., Feudel, U., Grebogi, C.: Preference of attractors in noisy multistable systems. Physical Review E **59**(5), 5253 (1999)
10. Kuznetsov, Y.A.: Elements of applied bifurcation theory, vol. 112. Springer Science & Business Media (2013)
11. Linz, S., Lücke, M.: Effect of additive and multiplicative noise on the first bifurcations of the logistic model. Physical Review A **33**(4), 2694 (1986)
12. Longtin, A.: Effects of noise on nonlinear dynamics. In: Nonlinear Dynamics in Physiology and Medicine, pp. 149–189. Springer (2003)
13. Medeiros, E.S., Caldas, I.L., Baptista, M.S., Feudel, U.: Trapping phenomenon attenuates the consequences of tipping points for limit cycles. Scientific reports **7**, 42,351 (2017)
14. Nordmark, A.B.: Non-periodic motion caused by grazing incidence in an impact oscillator. Journal of Sound and Vibration **145**(2), 279–297 (1991)
15. Nordmark, A.B.: Universal limit mapping in grazing bifurcations. Physical review E **55**(1), 266 (1997)
16. Nusse, H.E., Ott, E., Yorke, J.A.: Border-collision bifurcations: An explanation for observed bifurcation phenomena. Physical Review E **49**(2), 1073 (1994)
17. Piiroinen, P.T., Virgin, L.N., Champneys, A.R.: Chaos and period-adding; experimental and numerical verification of the grazing bifurcation. Journal of Nonlinear Science **14**(4), 383–404 (2004)
18. Rajasekar, S.: Controlling of chaotic motion by chaos and noise signals in a logistic map and a bonhoeffer–van der pol oscillator. Physical Review E **51**(1), 775 (1995)
19. Simpson, D.J., Hogan, S.J., Kuske, R.: Stochastic regular grazing bifurcations. SIAM Journal on Applied Dynamical Systems **12**(2), 533–559 (2013)
20. Simpson, D.J.W., Kuske, R.: The influence of localized randomness on regular grazing bifurcations with applications to impacting dynamics. Journal of Vibration and Control p. 1077546316642054 (2016)
21. de Souza, S.L., Batista, A.M., Caldas, I.L., Viana, R.L., Kapitaniak, T.: Noise-induced basin hopping in a vibro-impact system. Chaos, Solitons & Fractals **32**(2), 758–767 (2007)
22. de Souza, S.L., Caldas, I.L., Viana, R.L., Batista, A.M., Kapitaniak, T.: Noise-induced basin hopping in a gearbox model. Chaos, Solitons & Fractals **26**(5), 1523–1531 (2005)
23. Staunton, E.J., Piiroinen, P.T.: Noise and multistability in the square root map. Physica D: Nonlinear Phenomena **380-381**, 31 – 44 (2018). DOI https://doi.org/10.1016/j.physd.2018.06.002. URL `http://www.sciencedirect.com/science/article/pii/S0167278918300940`
24. Webber, J.B.W.: A bi-symmetric log transformation for wide-range data. Measurement Science and Technology **24**(2), 027,001 (2012)
25. Wiggins, S.: Introduction to applied nonlinear dynamical systems and chaos, vol. 2. Springer Science & Business Media (2003)